Bandpass Signal Design for Passive Time Delay Estimation

Jeffrey A. Nanzer
Michigan State University
428 S. Shaw Lane, East Lansing, MI 48824
Email: nanzerje@msu.edu

Matthew D. Sharp
Johns Hopkins Univ. Applied Physics Laboratory
11100 Johns Hopkins Road, Laurel, MD 20723
Email: Matthew.Sharp@jhuapl.edu

D. Richard Brown III
Worcester Polytechnic Institute
100 Institute Rd, Worcester, MA 01609
Email: drb@wpi.edu

***Abstract*—This paper analyzes the performance of passive time delay estimation with bandpass signals and generalizes the results of Weiss and Weinstein by considering a more general bandpass signal model with a parameter that allows for increasing the mean-squared bandwidth of the bandpass signal with respect to conventional flat bandpass signals. Analysis of the modified Ziv-Zakai lower bound shows (i) performance is typically improved at moderate to high signal to noise ratios due to the increased mean-squared bandwidth of the split bandpass signal but (ii) performance is typically worse at moderate to low signal to noise ratios due to increased ambiguities.**

***Index Terms*—time delay estimation, bandpass signals, maximum likelihood estimation**

I. Introduction

This paper considers the effect of bandpass signal design on the performance of passive time delay estimation. Fundamental limitations of passive time delay estimation for narrow-band and wide-band systems were studied in [1] and [2], respectively. While this work was based on a tight lower bound called the "modified Ziv-Zakai lower bound" which can be generally applied to any signal used for delay estimation, the analysis in [1], [2] focused primarily on spectrally flat bandpass signals with constant signal-to-noise ratio (SNR) over the band of interest such that

$$\mathsf{SNR}(\Omega) = \begin{cases} \mathsf{SNR} & |\Omega \pm \Omega_0| \leq W/2 \\ 0 & \text{otherwise.} \end{cases} \tag{1}$$

where Ω_0 is the carrier frequency (rad/sec) and W is the bandwidth (rad/sec) of the bandpass signal, respectively. Under this assumption, Weiss and Weinstein derived several elegant results including SNR thresholds that divide passive time delay estimation performance into three distinct operating regimes: (i) the the "no-information" regime with performance governed by *a priori* delay knowledge at low SNRs, (ii) the "ambiguity-dominated" regime with performance governed by the Barankin bound at moderate SNRs, and (iii) the "ambiguity-free" regime with performance governed by the Cramer-Rao lower bound at high SNRs. These regimes are notionally illustrated in Fig. 1.

The radar literature has also considered the fundamental limitations of time delay estimation, primarily focusing on the ambiguity-dominated regime [3], [4]. A well-known result states that the mean-squared error of time delay estimates is lower bounded by

$$\sigma^2 \geq \frac{1}{2\beta^2 \mathcal{E}/N_0} \tag{2}$$

where $\mathcal{E}/N_0$ is the post-integration SNR and

$$\beta^2 = \frac{\int_{-\infty}^{\infty} (2\pi f)^2 |S(f)|^2 \, df}{\int_{-\infty}^{\infty} |S(f)|^2 \, df} \tag{3}$$

This material is based upon work supported by the Naval Sea Systems Command under Contract No. N00024-13-D-6400, Task Order #0022 and by the National Science Foundation awards CCF-1302104 and CCF-1319458. Distribution Statement A — Approved for Public Release; Distribution Unlimited

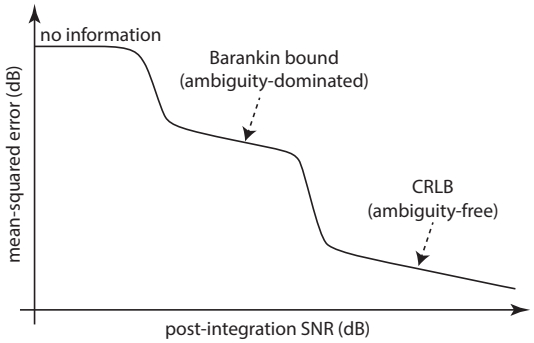

Fig. 1. Three operating regimes of passive time-delay estimation.

is the mean-squared bandwidth of the signal used for delay estimation where $f = \frac{\Omega}{2\pi}$. For a signal with a flat spectrum on $\Omega \in [-W/2, W/2]$ and zero otherwise, it can be straightforwardly verified that $\beta^2 = W^2/12$. Denoting T as the signal duration and $R = \left(\frac{WT}{2\pi}\right) \mathsf{SNR} = \mathcal{E}/N_0$ as the post-integration SNR for the flat bandpass signals in (1), we can rewrite (2) as

$$\sigma^2 \geq \frac{6}{W^2 R} \tag{4}$$

which is consistent with the Barankin bound in [1], [2] for post-integration SNRs in the ambiguity-dominated regime.

The general result in (2) naturally suggests that delay estimation performance can be improved by increasing the mean-squared bandwidth β^2. This can be achieved in the context of [1], [2] by simply increasing the bandwidth W. Increasing the bandwidth of the delay estimation signal may not be possible in some circumstances, however. In a setting where W is considered to fixed, one can still increase the mean-squared bandwidth with respect to the flat bandpass signals considered in [1], [2] by pushing the spectral content of the delay estimation signal to the extents of the available spectrum. In the limit, by transmitting tones at $\Omega \in \{-\Omega_0 \pm W/2, \Omega_0 \pm W/2\}$, the mean-squared bandwidth becomes $\beta^2 \to W^2/4$ and the lower bound on the delay estimation MSE improves by a factor of 3.

The primary question we consider in this paper is, given a fixed carrier frequency Ω_0 and signal bandwidth W, how does the mean-squared bandwidth β^2 affect the overall delay estimation performance in all three regimes shown in Fig. 1? Based on (2), we can expect the performance to improve in at least some portion of the ambiguity-dominated regime. But what are the tradeoffs, how are the transition regions affected, and how is the performance affected in the ambiguity-free and no-information regimes?

To answer these questions, we analyze the delay estimation performance of "split bandpass" signals shown in Fig. 2. These signals can be considered a generalization of the signals considered in [1], [2] and have an additional parameter $B \in (0, W/2]$ that allows control of

the mean-squared bandwidth of the signal. Note that the spectrum of the split bandpass signal is identical to the spectrum of the bandpass signals considered in [1], [2] when $B = W/2$. By decreasing B while holding W and the time-bandwidth product $2BT$ fixed, we can analyze the effect of increasing the mean-squared bandwidth on the MSE of delay estimation relative to the conventional flat bandpass signals in (1) over all three operating regimes.

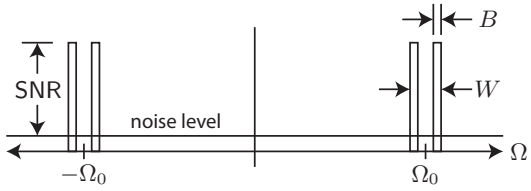

Fig. 2. "Split bandpass" spectrum.

Using the modified Ziv-Zakai lower bound, our results show that decreasing B typically achieves two effects: (i) it improves the MSE over a certain range of post-integration SNRs in the ambiguity-dominated regime and (ii) it pushes the transition to from the ambiguity-dominated regime to the the ambiguity-free regime in Fig. 1 left so that *the CRLB is achieved at lower post-integration SNRs* than with signals of the form in (1). These performance gains come with a tradeoff, however. For a certain range of low to moderate post-integration SNRs, the delay estimation performance of signals with increased mean-squared bandwidth can be considerably worse than the Barankin bound in (4) for signals of the form of (1). Moreover, choosing very small values for B (effectively maximizing the mean-squared bandwidth) leads to generally worse delay estimation performance except at very high post-integration SNRs. Intuitively, this is caused by the increased ambiguities inherent in split bandpass signals with small B. Hence, the applicability of split bandpass signals for passive delay estimation is primarily for systems with controlled moderate to high post-integration SNRs.

Applications for these results include ranging [5], synchronization [6], [7], and distributed wireless communication systems including distributed beamforming [8], [9] and distributed nullforming [10].

II. Modified Ziv-Zakai Lower Bound

The results in this paper comparing the delay estimation performance with conventional flat bandpass signals and split bandpass signals rely primarily on the "modified Ziv-Zakai" lower bound derived in [1], [2]. The modified Ziv-Zakai lower bound is given as

$$\sigma^2 \geq \frac{1}{D}\int_0^D xG[(D-x)P_e(x)]\,dx. \tag{5}$$

In (5), the term σ^2 denotes the delay estimation MSE, D denotes the maximum delay (signals are known *a priori* to arrive with a delay bounded in $[0, D]$), $P_e(x)$ is the minimum probability of error (achievable by a likelihood ratio test) for deciding between delay τ_0 and delay τ_1 where $\tau_1 - \tau_0 = x$, and

$$G[f(x)] = \max_{x \leq t \leq D} f(t) \tag{6}$$

is an operator that fills in the valleys of the function $f(x)$ so that $G[f(x)]$ is monotonically decreasing. The bound in (5) is general: there are no assumptions about the underlying signals.

To facilitate analysis, we assume the time-bandwidth product of the delay estimation signal is significantly larger than 1. Under this assumption, it was shown in [1], [2] that

$$P_e(x) \geq \overline{P}_e(x) = \exp\{-d(x)\} \cdot Q\left(\sqrt{c(x)}\right)$$

where $Q(\cdot)$ is the standard Q-function tail probability of the Gaussian distribution and

$$c(x) := \frac{T}{\pi}\int_0^\infty \mathsf{SNR}(\Omega)\sin^2(\Omega x/2)\,d\Omega \tag{7}$$

$$d(x) := \frac{T}{4\pi}\int_0^\infty \left[\mathsf{SNR}(\Omega)\sin^2(\Omega x/2)\right]^2\,d\Omega \tag{8}$$

Note that the integrals in (7) and (8) are both definite under the conventional bandpass and split bandpass signal models since both models have finite spectral support. The following sections analyze (7) and (8) for the conventional flat bandpass and split bandpass system models, respectively.

1) Conventional Flat Bandpass Signal Model: The conventional flat bandpass signal model is comprehensively analyzed in [1], [2]. We will summarize just the main results here to provide context for the analysis of the split bandpass model in the next section.

Since the conventional bandpass signal model specifies a constant $\mathsf{SNR}(\Omega)$ in the passband according to (1), it is straightforward to calculate.

$$c_{\text{flat}}(x) = R\left(1 - S_W(x/2)\cos(\Omega_0 x)\right)$$

$$d_{\text{flat}}(x) = \frac{\pi R^2}{8WT}\left(3 - 4S_W(x/2)\cos(\Omega_0 x) + S_W(x)\cos(2\Omega_0 x)\right)$$

with R denoting the post-integration SNR and $S_W(x) := \frac{\sin(Wx)}{Wx}$.

The results in [1], [2] are facilitated by analyzing $c_{\text{flat}}(x)$ and $d_{\text{flat}}(x)$ in two specific cases: (i) when x is close to zero and (ii) when $x = x_n = \frac{2\pi}{\Omega_0}n$ for integer n. In the former case, Maclaurin series approximations can be applied to write

$$c_{\text{flat}}(x) \approx R\frac{\Omega_0^2}{2}x^2 = c^2x^2 \quad \text{(small } x\text{)}$$

$$d_{\text{flat}}(x) \approx R^2\frac{2\pi}{8WT}\frac{\Omega_0^4}{4}x^4 = d^4x^4 \quad \text{(small } x\text{)}$$

In the latter case, when $x = x_n = \frac{2\pi}{\Omega_0}n$, the $\cos(\Omega_0 x)$ and $\cos(2\Omega_0 x)$ terms become one in the expressions for $c_{\text{flat}}(x)$ and $d_{\text{flat}}(x)$. Using the bounds $x - \frac{x^3}{3} \leq \sin(x) \leq x$, we can write

$$c_{\text{flat}}(x_n) \leq \frac{W^2}{24}Rx_n^2 = \tilde{c}^2x_n^2 \tag{9}$$

$$d_{\text{flat}}(x_n) \leq \frac{W^3\pi}{T\cdot 15\cdot 2^6}R^2x_n^4 = \tilde{d}^4x_n^4 \tag{10}$$

After several additional approximations (the reader is referred to Appendix C of [2] for the full details), Weiss and Weinstein present the delay estimation MSE lower bound

$$\begin{aligned}\sigma^2 \geq\ & \frac{1}{c^2}\int_0^{\tilde{c}T_0} x\exp\left\{-(dx/c)^4\right\}Q(x)\,dx \\ & + \frac{1}{\tilde{c}^2}\int_{\tilde{c}T_0}^{\sqrt{R}} x\exp\left\{-(\tilde{d}x/\tilde{c})^4\right\}Q(x)\,dx + \frac{D^2}{6}Q(\sqrt{R})\end{aligned} \tag{11}$$

where $T_0 = \frac{2\pi}{\Omega_0}$. Assuming a sufficiently large time-bandwidth product, the three regimes shown in Fig. 1 can be characterized directly from this last expression as follows:

1) When $R \ll 1$, the quantity $\tilde{c}T_0 = \pi\frac{W}{\Omega_0}\sqrt{\frac{R}{6}}$ is close to zero and the dominant term is the third term. In this case, we have
$$\sigma^2 \approx \frac{D^2}{6}Q(\sqrt{R}) \approx \frac{D^2}{12} \tag{12}$$
which corresponds to the "no information" bound.
2) When $1 \ll R \ll \frac{\Omega_0^2}{W^2}$, the quantity $\tilde{c}T_0 = \pi\frac{W}{\Omega_0}\sqrt{\frac{R}{6}}$ is still small. The first and third terms are negligible and the dominant

term is the second term. In this case, we have

$$\begin{aligned}\sigma^2 &\approx \frac{1}{\tilde{c}^2}\int_{\tilde{c}T_0}^{\sqrt{R}} x\exp\left\{-(\tilde{d}x/\tilde{c})^4\right\}Q(x)\,dx\\ &\approx \frac{24}{W^2R}\int_{\tilde{c}T_0}^{\infty} xQ(x)\,dx\\ &\approx \frac{24}{W^2R}\cdot\frac{1}{2}Q\left(\tilde{c}T_0\right)\\ &\approx \frac{6}{W^2R}\end{aligned}$$

which corresponds to the Barankin bound in the ambiguity-dominated regime and is consistent with (4).

3) When $R \gg \frac{\Omega_0^2}{W^2}$, the quantity $\tilde{c}T_0 = \pi\frac{W}{\Omega_0}\sqrt{\frac{R}{6}}$ is large and the dominant term is the first term. In this case, we have

$$\begin{aligned}\sigma^2 &\approx \frac{1}{c^2}\int_{0}^{\tilde{c}T_0} x\exp\left\{-(dx/c)^4\right\}Q(x)\,dx\\ &\approx \frac{2}{\Omega_0^2R}\int_{0}^{\infty} xQ(x)\,dx\\ &\approx \frac{1}{2\Omega_0^2R}\end{aligned}$$

which corresponds to the ambiguity-free regime and the CRLB.

The critical transition from the ambiguity-dominated regime to the ambiguity-free regime approximately begins when $Q(\tilde{c}T_0) = 1/4$ and approximately ends when $\frac{12}{W^2R}Q(\tilde{c}T_0) = \frac{1}{2\Omega_0^2R}$. Substituting $\tilde{c}$ from (9), we can write the approximate beginning and end of the transition region respectively as

$$R'_{\text{flat}} = \frac{6(Q^{-1}(1/4))^2}{\pi^2}\left(\frac{\Omega_0}{W}\right)^2 = f'(\Omega_0/W) \tag{13}$$

$$R''_{\text{flat}} = \frac{6}{\pi^2}\left(\frac{\Omega_0}{W}\right)^2\left[Q^{-1}\left(\frac{W^2}{24\Omega_0^2}\right)\right]^2 = f''(\Omega_0/W) \tag{14}$$

As shown in Section IV, these approximate beginning and ending points of the critical transition region tend to be quite accurate, at least in the cases tested in this paper.

2) Split Bandpass Signal Model: This section leverages the analysis in the previous section to characterize the performance limits of the split bandpass signal model and determine the tradeoffs in increasing the mean squared bandwidth by pushing the spectral content of the signal to the extents of the available spectrum.

For the split bandpass signal model shown in Fig. 2, $\mathsf{SNR}(\Omega)$ for $\Omega \geq 0$ is non-zero and constant on $\Omega \in [\Omega_0 - W/2, \Omega_0 - W/2 + B] \cup [\Omega_0 + W/2 - B, \Omega_0 + W/2]$. Straightforward calculations result in

$$\begin{aligned}c_{\text{split}}(x) &= R\left(1 - S_B(x/2)\cos((W-B)x/2)\cos(\Omega_0 x)\right)\\ d_{\text{split}}(x) &= \frac{\pi R^2}{16BT}\Big[3 - 4S_B(x/2)\cos((W-B)x/2)\cos(\Omega_0 x)\\ &\qquad + S_B(x)\cos((W-B)x)\cos(2\Omega_0 x)\Big]\end{aligned}$$

with $S_B(x) := \frac{\sin(Bx)}{Bx}$ and $R = \frac{2BT}{2\pi}\mathsf{SNR}$.

For x close to zero, we can use Maclaurin series approximations to write

$$\begin{aligned}c_{\text{split}}(x) &\approx R\frac{\Omega_0^2}{2}x^2 = c^2x^2\\ d_{\text{split}}(x) &\approx R^2\frac{2\pi}{16BT}\frac{\Omega_0^4}{4}x^4 = d^4x^4\end{aligned}$$

When $x = x_n = \frac{2\pi}{\Omega_0}n$, we can use the bounds $\sin(x) \geq x - \frac{x^3}{3}$ and $\cos(x) \geq 1 - \frac{x^2}{2}$ to write

$$\begin{aligned}c_{\text{split}}(x_n) &\leq R\left(1 - \left(1 - \frac{B^2x_n^2}{24}\right)\left(1 - \frac{(W-B)^2x_n^2}{8}\right)\right)\\ &= R\left(\left(\frac{B^2 + 3(W-B)^2}{24}\right)x_n^2 - \frac{3B^2(W-B)^2}{(24)^2}x_n^4\right)\\ &\leq R\left(\frac{B^2 + 3(W-B)^2}{24}\right)x_n^2\\ &= R\frac{\beta^2}{2}x_n^2\\ &= \tilde{c}^2x_n^2\end{aligned} \tag{15}$$

where the result on line 4 follows from the fact that the mean-squared bandwidth $\beta^2 = \frac{B^2+3(W-B)^2}{12}$ for the split bandpass signal model. A similar analysis can be performed on $d_{\text{split}}(x)$ at $x = x_n$ to write

$$d_{\text{split}}(x_n) \leq \frac{(W^5 + 8(W/2-B)^5)\pi}{TB^2\cdot 15\cdot 2^8}R^2x_n^4 = \tilde{d}^4x_n^4.$$

All of these results can be shown to agree with the results for the conventional flat bandpass signal model when $B = W/2$.

Assuming a sufficiently large time-bandwidth product, the analysis and approximations in the previous section for the conventional flat bandpass signal model revealed that the operating regimes are only a function of c and $\tilde{c}$. Note that c is identical for conventional flat bandpass and split bandpass signal models but $\tilde{c}$ differs in that $\frac{W^2}{12}$ is replaced by β^2. Hence, the results in the previous section for the conventional bandpass signal model can be translated to the split bandpass signal model by replacing $\frac{W^2}{12}$ with β^2. The operating regimes and achieved MSE in these regimes are summarized as:

1) $R \ll 1$: $\sigma^2 \approx \frac{D^2}{12}$ (same as conventional flat bandpass).
2) $1 \ll R \ll \frac{\Omega_0^2}{12\beta^2}$: $\sigma^2 \approx \frac{1}{2\beta^2R}$.
3) $R \gg \frac{\Omega_0^2}{12\beta^2}$: $\sigma^2 \approx \frac{1}{2\Omega_0^2R}$ (same as conventional flat bandpass).

Similarly, the critical transition region approximate beginning and end points from ambiguity-dominated to ambiguity-free operation can be written as

$$R'_{\text{split}} = f'\left(\frac{\Omega_0}{\sqrt{12}\beta}\right) \tag{16}$$

$$R''_{\text{split}} = f''\left(\frac{\Omega_0}{\sqrt{12}\beta}\right). \tag{17}$$

Defining the relative mean-squared bandwidth $\alpha := \frac{\beta^2}{W^2/12} \in [1, 3)$, we can compute the relative SNR of the beginning and end of the critical transition region for split bandpass signals with respect to conventional bandpass signals as

$$\begin{aligned}\frac{R'_{\text{split}}}{R'_{\text{flat}}} &= \frac{1}{\alpha}\\ \frac{R''_{\text{split}}}{R''_{\text{flat}}} &= \frac{1}{\alpha}\left(\frac{Q^{-1}\left(\alpha\frac{W^2}{24\Omega_0^2}\right)}{Q^{-1}\left(\frac{W^2}{24\Omega_0^2}\right)}\right)^2.\end{aligned}$$

As a numerical example, suppose we have a fractional bandwidth $\frac{W}{\Omega_0} = \frac{1}{100}$ and a split bandpass signal with $\frac{B}{W} = \frac{1}{10}$. The relative mean-squared bandwidth can be computed as $\alpha = 2.44$, which implies that the start of the critical transition region is shifted to the left by approximately 3.9 dB and the end of the critical transition region is shifted to the left by approximately 4.3 dB. This example shows that, in addition to the expected performance improvement of split bandpass signals in the ambiguity-dominated regime, the

transition to the ambiguity-free regime can occur at lower post-integration SNRs than with conventional bandpass signals. This effect will be numerically confirmed in Section IV using the modified Ziv-Zakai lower bound and Monte-Carlo tests of a maximum likelihood delay estimator.

Numerical tests show that the ambiguity-dominated regime for split bandpass signals actually has two sub-regimes not revealed by the prior analysis. To better understand these sub-regimes, we can assume the carrier at Ω_0 provides no useful information and consider delay estimation in regime (2) with a downmixed version of the split bandpass signal such that

$$\mathsf{SNR}(\Omega) = \begin{cases} \mathsf{SNR} & |\Omega \pm \Omega_0'| \le B/2 \\ 0 & \text{otherwise.} \end{cases} \tag{18}$$

with $\Omega_0' = \frac{W-B}{2}$. Observe that this downmixed signal is a conventional flat bandpass signal with bandwidth B and carrier frequency $(W-B)/2$. The regimes follow directly from the analysis in Section II-1 as:

1) $R \ll 1$: $\sigma^2 \approx \frac{D^2}{12}$.
2) $1 \ll R \ll \frac{3(W-B)^2}{B^2}$: $\sigma^2 \approx \frac{6}{B^2 R}$.
3) $R \gg \frac{3(W-B)^2}{B^2}$: $\sigma^2 \approx \frac{2}{(W-B)^2 R}$.

The implicit assumption $\frac{3(W-B)^2}{B^2} \gg 1$ implies that the mean squared bandwidth can be approximated as

$$\beta^2 = \frac{B^2 + 3(W-B)^2}{12} \approx \frac{(W-B)^2}{4}.$$

With this approximation, observe that regime (3) of the downmixed signal model is consistent with the results in regime (2) for the split bandpass signal model. Regime (2) of the downmixed signal model, however, reveals the additional ambiguities caused by narrowing the bandwidth B of the split bandpass signal: if the post-integration SNR is not sufficiently high, performance is dominated by B-ambiguities (with MSE $\frac{6}{B^2 R}$) rather than β-ambiguities (with MSE $\frac{2}{(W-B)^2 R} \approx \frac{1}{2\beta^2 R} \ll \frac{6}{B^2 R}$). The transition from the B-ambiguity-dominated regime to the β-ambiguity dominated regime begins at $f'((W-B)/(2B))$ and ends at $f''((W-B)/(2B))$, where f' and f'' are defined in (13) and (14), respectively.

To fully characterize the performance limits of delay estimation with split bandpass signals, we summarize the preceding analysis by listing the operating regimes and the transition regions as

$$\sigma^2 \approx \begin{cases} \frac{D^2}{12} & R < 0.4613 \\ \text{transition} & 0.4613 < R < R_2 \\ \frac{6}{B^2 R} & R_2 < R < f'((W-B)/(2B)) \\ \text{transition} & f'((W-B)/(2B)) < R < f''((W-B)/(2B)) \\ \frac{1}{2\beta^2 R} & f''((W-B)/(2B)) < R < f'(\Omega_0/(\sqrt{12}\beta)) \\ \text{transition} & f'(\Omega_0/(\sqrt{12}\beta)) < R < f''(\Omega_0/(\sqrt{12}\beta)) \\ \frac{1}{2\Omega_0^2 R} & R > f''(\Omega_0/(\sqrt{12}\beta)) \end{cases}$$

where R_2 is the larger solution to the transcendental equation $R_2 Q(R_2) = \left(\frac{6}{BD}\right)^2$. If BD is small, a solution to this equation may not exist, which implies that the B-ambiguity-dominated regime transitions directly into the no-information regime. Tabulated values for R_2 can be found in [2].

III. Maximum Likelihood Estimator

To confirm the bounds and approximations derived in the previous section are accurate indicators of the delay estimation performance that can be achieved in practice, this section describes an implementation of a maximum likelihood delay estimator. Numerical results in Section IV verify this delay estimator achieves a MSE close to the bounds derived in the previous section in the cases considered.

Given a template signal $s(t)$ and an observation

$$y(t) = as(t-\tau) + w(t)$$

where $0 \le \tau \le D$ is a bounded delay and $w(t)$ is noise with flat spectrum in the support of the template signal's spectrum, it is well-known, e.g., [11], that the maximum likelihood estimate of τ can be calculated by correlating the template signal $s(t)$ with the observation $y(t)$ and setting $\hat{\tau}$ equal to the peak of the correlation, i.e.,

$$\hat{\tau} = \arg \max_{0 \le \nu \le D} \int s(t-\nu) y(t)\, dt. \tag{19}$$

In practice, we can't compute (19) directly since we typically have a discrete-time observation with some sampling rate f_s rather than a continuous-time observation. Instead, we can compute

$$\hat{k} = \arg \max_{-\frac{D}{2T_s} \le \ell \le \frac{D}{2T_s}} \sum_k s[k-\ell] y[k] \tag{20}$$

where $y[k] = y(kT_s)$ and $s[k-\ell] = s((k-\ell)T_s)$ with $T_s = \frac{1}{f_s}$. The delay estimate from the discrete-time observation is then

$$\hat{\tau} = \hat{k} T_s. \tag{21}$$

In general, the discrete-time correlation in (20) is an unsatisfactory substitute for the continuous-time correlation in (19) because (i) the sampling period effectively quantizes the delay estimates and sets a floor on the achievable performance of the delay estimator and (ii) the discrete-time delay estimate may select an incorrect correlation peak in signals with quasi-periodic correlations even at infinite SNR since the samples may miss the actual peaks of the correlation function. These problems can be overcome to some extent by oversampling or interpolating the discrete-time signal, but this can significantly increase the computational complexity of the delay estimator. In this section, we describe an alternative approach to maximum likelihood delay estimation with discrete-time signals when the template signal is a modulated baseband signal of the form

$$s(t) = \cos(\Omega_0 t) u(t)$$

where $u(t)$ is a bandlimited signal such that $U(\Omega) = 0$ for all $|\Omega| \ge \Omega_0$.

The template signal in discrete time can be expressed as

$$s[k] = \left[\cos(\Omega_0 t) u(t)\right]_{t=kT_s} = \cos(\omega_0 k) u[k]$$

where $\omega_0 = \Omega_0 T_s$ is the normalized carrier frequency in radians/sample

The discrete-time observation with unknown delay $0 \le \tau \le D$ can be expressed as

$$\begin{aligned} y[k] &= \left[\cos(\Omega_0(t-\tau)) u(t-\tau)\right]_{t=kT_s} \\ &= \cos(\omega_0(k - \tau f_s)) u(kT_s - \tau) \end{aligned}$$

for $k = 0, \ldots, K-1$.

The discrete-time delay estimate $\hat{k}$ is computed according to (20). To refine the delay estimate, we define

$$\begin{aligned} s_i[k,\ell] &= \cos(\omega_0(k-\ell)) u[k-\ell] \\ s_q[k,\ell] &= \sin(\omega_0(k-\ell)) u[k-\ell]. \end{aligned}$$

Using $\hat{k}$ from (20), we can compute

$$z_i[\hat{k}] = \sum_{k=0}^{K-1} y[k] s_i[k,\hat{k}] \approx \frac{\cos(\omega_0(\tau f_s - \hat{k}))}{2} \sum_{k=0}^{K-1} u(kT_s - \tau) u[k - \hat{k}]$$

where the approximation results from the the fact that $\sum_{k=0}^{K-1} \cos(\omega_0(2k - \tau f_s - \hat{k}))u(kT_s - \tau)u[k - \hat{k}] \approx 0$. Similarly, we can calculate

$$z_q[\hat{k}] = \sum_{k=0}^{K-1} y[k]s_q[k, \hat{k}] \approx \frac{\sin(\omega_0(\tau f_s - \hat{k}))}{2} \sum_{k=0}^{K-1} u(kT_s - \tau)u[k - \hat{k}]$$

We can then compute

$$\begin{aligned} \theta &= \tan^{-1}\left(\frac{z_q[\hat{k}]}{z_i[\hat{k}]}\right) \\ &= \tan^{-1}\left(\frac{\sin(\omega_0(\tau f_s - \hat{k}))}{\cos(\omega_0(\tau f_s - \hat{k}))}\right) \\ &= \omega_0(\tau f_s - \hat{k}). \end{aligned} \tag{22}$$

The refined delay estimate can then be computed as

$$\hat{\tau} = \left(\hat{k} + \frac{\theta}{\omega_0}\right) T_s \tag{23}$$

where θ is calculated according to (22) and $\hat{k}$ is from (20).

A remark: Note that a four-quadrant arctangent will result in $-\pi \leq \theta \leq \pi$. Also note that $\omega_0 < \pi$ if the sampling frequency is chosen to avoid aliasing. Hence, the "delay refinement" $\frac{\theta}{\omega_0}$ must fall in the interval

$$\frac{\theta}{\omega_0} \in \left[\frac{-\pi}{\omega_0}, \frac{\pi}{\omega_0}\right] \supseteq [-1, +1].$$

In other words, the delay refinement can (at a minimum) adjust the discrete-time delay estimate $\hat{k}$ by a full sample in either direction. The adjustment can be even larger if the sampling rate is selected so that the normalized carrier frequency $\omega_0 = \frac{\Omega_0}{f_s}$ is small. In any case, if the discrete-time delay estimate $\hat{k}$ is sufficiently close to τf_s such that

$$|\hat{k} - \tau f_s| \leq \frac{\pi}{\omega_0} \tag{24}$$

then the refinement can form an accurate estimate of the true delay τ. If, on the other hand, $\hat{k}$ is such that (24) is not satisfied, then the refinement step can not result in an accurate estimate of the true delay τ.

To address this problem, we can consider a modification of the procedure above to provide N distinct candidate discrete-time delays $\hat{k}_1, \ldots \hat{k}_N$. The number of candidate delays is a parameter that can be selected to allow the maximum likelihood delay estimator to find a discrete-time delay estimate sufficiently close to the actual delay without excessive additional computational complexity. This number can be small if the correlation function does not have strong periodicity but should be larger when the correlation function is quasi-periodic. A delay refinement is then computed for each of these candidate discrete-time delays, resulting in N candidate continuous-time delay estimates $\hat{\tau}_1, \ldots, \hat{\tau}_N$. The maximum likelihood delay estimate is then selected from the candidate delay estimates according to

$$\hat{\tau} = \arg \max_{\nu \in \{\hat{\tau}_1, \ldots, \hat{\tau}_N\}} \sum_k s(kT_s - \nu)y[k]. \tag{25}$$

Note that computation of (25) requires re-calculation of the known template signal $s(t)$ at each of the candidate continuous-time delays.

IV. Numerical Results

This section presents numerical results verifying the analysis in Section II and also demonstrating the efficacy of the maximum likelihood delay estimator developed in Section III.

Figure 3 shows the directly integrated modified Ziv-Zakai lower bound, performance limits in each operating regime, and the achieved maximum likelihood delay estimator performance for a conventional flat bandpass signal model with carrier frequency $\Omega_0 = 2\pi \cdot 4000$, fractional bandwidth $\frac{W}{\Omega_0} = \frac{1}{100}$, time-bandwidth product $\frac{TW}{2\pi} = 50$, and maximum delay $D = 10^5 \cdot T_0$. Observe that the directly integrated modified Ziv-Zakai lower bound closely follows the three regimes predicted by the analysis. The maximum likelihood delay estimator also closely follows the bound. The delay estimator with discrete-time correlation (no refinement) clearly shows the expected error floor caused by quantization of the delay estimates at the simulation sampling rate $f_s = 16$ kHz. The effect of multiple candidate delays on the performance of the delay estimator is only observed in the critical transition region. With 2 or more candidate delays, the maximum likelihood delay estimator reaches the ambiguity-free regime at a slightly lower post-integration SNR than with a single candidate delay.

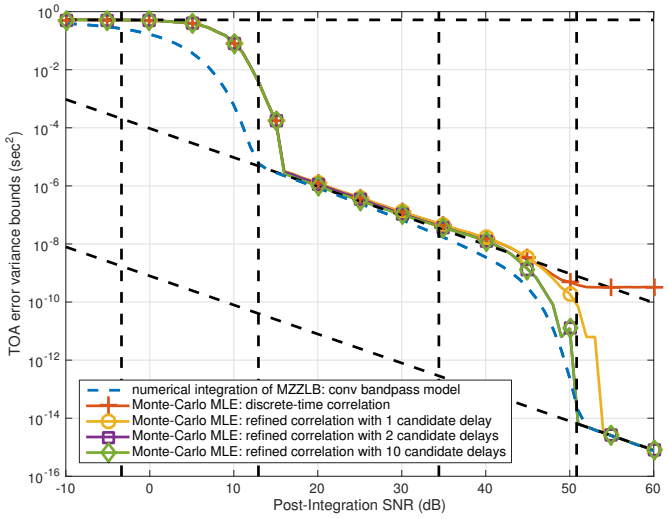

Fig. 3. Maximum likelihood delay estimation versus directly integrated modified Ziv-Zakai lower bound for a conventional flat bandpass signal with $\frac{W}{\Omega_0} = \frac{1}{100}$. Black dashed lines correspond to the thresholds of the transition regions and the performance in each regime as derived in Section II-1.

Figure 4 shows a similar result for the split bandpass signal model with identical parameters as Fig. 3 and $\frac{B}{W} = \frac{1}{10}$. The magenta dashed lines correspond to the thresholds of the transition regions and the performance in each regime as derived in Section II-2. The black dashed lines are copied from Fig. 3 for the conventional flat bandpass signal model for comparison. We see that the directly integrated modified Ziv-Zakai lower bound closely follows the regimes predicted by the analysis and the maximum likelihood delay estimator also closely follows the bound. As predicted by the analysis, we also see the two sub-regimes of the ambiguity-dominated regime and the transition from B-ambiguity-dominated to β-ambiguity dominated behavior between 25-30 dB post-integration SNR. Most importantly, we see that the split bandpass signal provides better performance than the conventional flat bandpass signal for delay estimation for post-integration SNRs between approximately 30 dB and 50 dB. The performance gains are significant especially in range of post-integration SNRs where the split bandpass signal operates in the ambiguity-free regime while the conventional flat bandpass signal is still in the ambiguity-dominated regime (approximately 45-50 dB post-integration SNR).

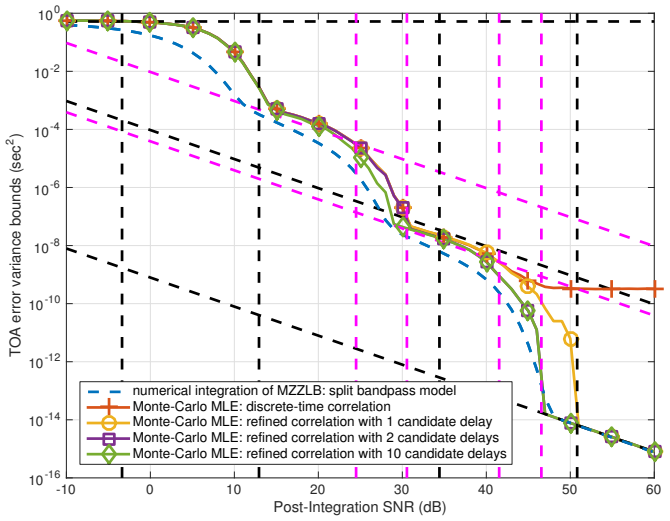

Fig. 4. Maximum likelihood delay estimation versus directly integrated modified Ziv-Zakai lower bound for a split bandpass signal with $\frac{W}{\Omega_0} = \frac{1}{100}$ and $\frac{B}{W} = \frac{1}{10}$. Magenta dashed lines correspond to the thresholds of the transition regions and the performance in each regime as derived in Section II-2.

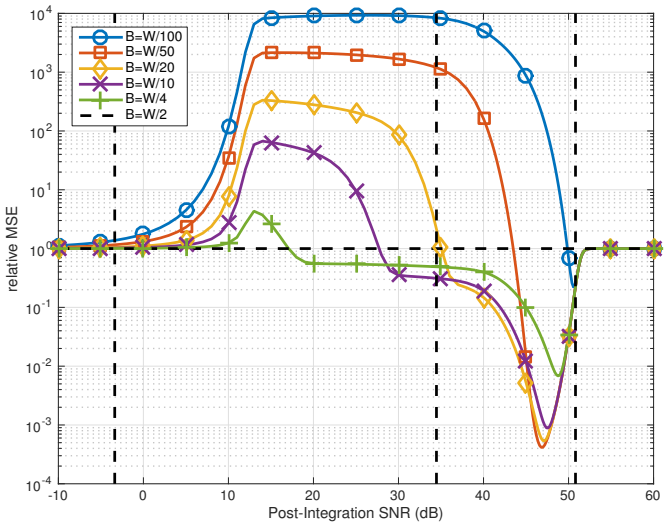

Fig. 5. Relative MSE of delay estimation using split bandpass signals for fractional bandwidth $\frac{W}{\Omega_0} = \frac{1}{100}$. Values less than one correspond to settings in which delay estimation with split bandpass signals outperforms delay estimation with conventional flat bandpass signals.

Figure 5 shows the relative delay estimation MSE of split bandpass signals with respect to conventional flat bandpass signals for $\frac{W}{\Omega_0} = \frac{1}{100}$. The relative MSE in these results is calculated by computing the ratio of directly integrated modified Ziv-Zakai lower bounds for the split bandpass and conventional flat bandpass signals. These results show that split bandpass signals can improve performance in the ambiguity-dominated regime with significant gains (exceeding three orders of magnitude in this example) at moderate to high SNRs near the transition to the ambiguity-free regime. The tradeoff, however, is that delay estimation performance can be significantly worse than conventional flat bandpass signals at moderate to low SNRs due to the B-ambiguity-dominated regime as discussed in Section II-2. As $\frac{B}{W}$ decreases, the mean-squared bandwidth β^2 increases, but the regime in which the split bandpass signal outperforms the conventional flat bandpass signal diminishes due to the increasing B-ambiguities. At very small values of $\frac{B}{W}$, the B-ambiguities dominate the performance except at very high and very low post-integration SNRs.

V. Conclusion

This paper analyzed the performance of passive time delay estimation with split bandpass signals and developed a discrete-time maximum likelihood delay estimator that achieves a MSE close to the performance bounds. Our analysis showed that split bandpass signals generally provide four regimes of operation: (i) no information, (ii) B-ambiguity-dominated, (iii) β-ambiguity-dominated, and (iv) ambiguity-free. By increasing the mean-squared bandwidth of the split bandpass signals and maintaining a fixed time-bandwidth product significantly larger than one, delay estimation performance is typically improved at moderate to high post-integration SNRs and the transition from ambiguity-dominated to ambiguity-free operation occurs at lower SNRs. The tradeoff, however, is that performance is typically worse at low SNR due to the increased ambiguities in the B-ambiguity-dominated regime. Our results can be considered a generalization of the analysis in [1], [2] and are consistent with the results of Weiss and Weinstein when $B = W/2$.

References

[1] A. Weiss and E. Weinstein, "Fundamental limitations in passive time delay estimation–Part I: Narrow-band systems," *Acoustics, Speech and Signal Processing, IEEE Transactions on*, vol. 31, no. 2, pp. 472 – 486, April 1983.

[2] E. Weinstein and A. Weiss, "Fundamental limitations in passive time-delay estimation–Part II: Wide-band systems," *Acoustics, Speech and Signal Processing, IEEE Transactions on*, vol. 32, no. 5, pp. 1064 – 1078, October 1984.

[3] P. Woodward, *Probability and information theory, with applications to radar*. New York, NY: McGraw-Hill, 1953.

[4] M. I. Skolnik, *Introduction to radar systems*. McGraw-Hill, 2001.

[5] J. Hodkin, K. Zilevu, M. Sharp, T. Comberiate, S. Hendrickson, M. Fitch, and J. Nanzer, "Microwave and millimeter-wave ranging for coherent distributed RF systems," in *Aerospace Conference, 2015 IEEE*, March 2015, pp. 1–7.

[6] P. Bidigare, U. Madhow, R. Mudumbai, and D. Scherber, "Attaining fundamental bounds on timing synchronization," in *Acoustics, Speech and Signal Processing (ICASSP), 2012 IEEE International Conference on*, Mar. 2012, pp. 5229–5232.

[7] M. Li, S. Gvozdenovic, A. Ryan, R. David, D.R. Brown III, and A. Klein, "A real-time implementation of precise timestamp-free network synchronization," Nov. 2015.

[8] R. Mudumbai, D.R. Brown III, U. Madhow, and H.V. Poor, "Distributed transmit beamforming: challenges and recent progress," *Communications Magazine, IEEE*, vol. 47, no. 2, pp. 102–110, February 2009.

[9] P. Bidigare, M. Oyarzun, D. Raeman, D. Cousins, D. Chang, R. O'Donnell, and D.R. Brown III, "Implementation and demonstration of receiver-coordinated distributed transmit beamforming across an ad-hoc radio network," in *Proc. of the 46th Asilomar Conf. on Signals, Systems, and Computers*, Pacific Grove, CA, November 4-7 2012, pp. 222–226.

[10] D.R. Brown III and R. David, "Receiver-coordinated distributed transmit nullforming with local and unified tracking," in *Proc. of the 39th International Conf. on Acoustics, Speech, and Signal Processing (ICASSP2014)*, Florence, Italy, May 4-9 2014.

[11] C. Knapp and G. Carter, "The generalized correlation method for estimation of time delay," *Acoustics, Speech and Signal Processing, IEEE Transactions on*, vol. 24, no. 4, pp. 320–327, Aug 1976.